

A Bifunctional Aggregation-Induced Emission Luminogen for Monitoring and Killing of Multidrug-Resistant Bacteria

Ying Li, Zheng Zhao, Jiangjiang Zhang, Ryan T. K. Kwok, Sheng Xie, Rongbing Tang, Yuexiao Jia, Junchuan Yang, Le Wang, Jacky W. Y. Lam, Wenfu Zheng,* Xingyu Jiang,* and Ben Zhong Tang*

Multidrug-resistant (MDR) bacteria pose serious threats to public health as there is currently a lack of effective and biocompatible drugs to kill MDR bacteria. Here, a bifunctional aggregation-induced emission luminogen (AIEgen), triphenylethylene-naphthalimide triazole (TriPE-NT), is reported, which is capable of both staining and killing Gram-positive (G+) and Gram-negative (G-) bacteria. The intrinsic fluorescence generating ability of the TriPE unit enables TriPE-NT to monitor the drug–bacteria interactions, meanwhile, the NT unit renders TriPE-NT the antibacterial activity. Furthermore, TriPE-NT can generate reactive oxygen species (ROS) under light irradiation and drastically enhance its antibacterial efficacy by photodynamic therapy against wild bacteria and clinical isolated MDR bacteria with a very low toxicity to mammalian cells. Moreover, the efficiency of TriPE-NT staining on bacteria closely correlates with its antibacterial efficacy. As an example of application, TriPE-NT is utilized in curing *Escherichia coli* (*E. coli*), MDR *E. coli*-, *Staphylococcus epidermidis* (*S. epidermidis*), and MDR *S. epidermidis*-infected wounds on rats with high efficacy and high safety. Thus, TriPE-NT can be used not only as a powerful antibiotic agent for treating MDR bacteria-infected diseases but also as a potential fluorescent agent for monitoring the bacterial infections and further exploring the related antibacterial mechanism.

1. Introduction

Multidrug-resistant (MDR) bacteria pose serious threats to public health due to the lack of biocompatible antibiotics that can effectively kill the MDR bacteria.^[1–4] With the emergence of drug-resistance against existing antibiotics, it is of utmost urgency to develop new therapeutic agents.

Photodynamic therapy (PDT) is a potential alternative to antibiotics to kill bacteria.^[5–7] In general, PDT employs photosensitizers (PSs) to absorb light and generate single excited state (S_1), the S_1 state can further transfer the energy to triplet excited state (T_1), which would sensitize the ambient triplet oxygen, resulting in formation of the destructive singlet oxygen or other reactive oxygen species (ROS).^[8,9] PDT can target both external and internal structures of bacteria, and not really requires the PSs to enter bacteria, thus, the sterilization mechanism of PDT is different from traditional antibiotics. Therefore, bacteria can hardly develop


Dr. Y. Li, Dr. Z. Zhao, Dr. R. T. K. Kwok, Dr. S. Xie, Dr. J. W. Y. Lam,
Prof. B. Z. Tang
Department of Chemical and Biological Engineering
Department of Chemistry
Hong Kong Branch of Chinese National Engineering Research
Center for Tissue Restoration and Reconstruction
Institute for Advanced Study
Division of Life Science
The Hong Kong University of Science and Technology
Clear Water Bay, Kowloon, Hong Kong 999077, China
E-mail: tangbenz@ust.hk

Dr. J. J. Zhang, R. B. Tang, Dr. Y. X. Jia, Dr. J. C. Yang, L. Wang,
Prof. W. F. Zheng, Prof. X. Y. Jiang
CAS Center for Excellence in Nanoscience
CAS Key Lab for Biological Effects of Nanomaterials and Nanosafety
National Center for NanoScience and Technology
BeiYiTiao, ZhongGuanCun, Beijing 100190, China
E-mail: zhengwf@nanoctr.cn; xingyujiang@nanoctr.cn

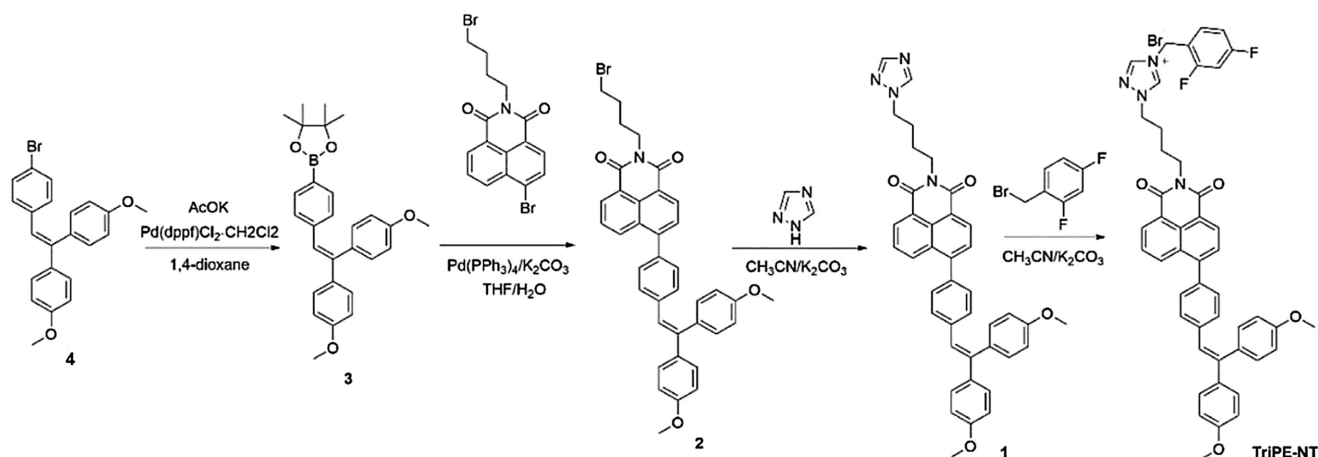
Prof. X. Y. Jiang
University of Chinese Academy of Science
Beijing 100049, China

Prof. B. Z. Tang
HKUST-Shenzhen Research Institute
No. 9 Yuexing 1st RD, South Area, Hi-tech Park, Nanshan, Shenzhen
518057, China

Prof. B. Z. Tang
NSFC Center for Luminescence from Molecular Aggregates
SCUT-HKUST Joint Research Laboratory
State Key Laboratory of Luminescent Materials and Devices
South China University of Technology
Guangzhou 510640, China

 The ORCID identification number(s) for the author(s) of this article can be found under <https://doi.org/10.1002/adfm.201804632>.

DOI: 10.1002/adfm.201804632



Scheme 1. Synthetic routes for TriPE-NT.

resistance to PDT.^[10] However, most of the PSs reported so far are hydrophobic and tend to form aggregates when they interact with bacteria in physiological hydrophilic conditions. Such molecular aggregation could cause the quenching of the singlet state, which thus quenches the fluorescence and also reduces ROS generation and compromises the effects of both imaging and therapy.^[11] In comparison with traditional PSs, organic luminogens with aggregation-induced emission characteristics are a class of molecules showing faint or no emission in solution, but enhanced emission upon aggregation.^[12,13] The unique aggregation lit-up fluorescence characteristic of AIEgens enables their extensive bioimaging applications.^[14–17] More importantly, some AIEgens were found to exhibit aggregation enhanced ROS generation property, suggesting their potential applications in image-guided PDT.^[18] Until now, several AIEgens have been reported for imaging or killing bacteria,^[19–21] however, these reported AIEgens mostly are monofunctional and their antibacterial ability are not systematically investigated. Liu and co-workers have explored the integration of ROS-generating AIEgen with commercial antibiotics, aiming at enhancing bacteria killing ability,^[19] however it showed limited antibiotic capability since it is well known that drugs are very sensitive to structural modifications. So, is it possible to integrate antibiotics with PDT to generate powerful novel superantibiotics to combat with bacteria or even MDR bacteria?

In this study, we designed a new class of antimicrobial agents (TriPE-NT) which connect an AIE unit triphenylethylene (TriPE) with naphthalimide triazole (NT). Azoles-substituted naphthalimide belong to an important class of antimicrobial agents.^[22–24] TriPE-substituted naphthalimide is designed as an effective AIEgen with ROS generation capability. It is of great interest and challenge for us to explore their combinational effects to generate new types of antimicrobial agents which can integrate the killing ability of both ROS and azoles. Furthermore, the intrinsic imaging ability of TriPE-NT enables it as an imaging tool to monitor the drug–bacteria interactions. The results indicated that TriPE-NT not only successfully maintained antibacterial function of azole, but also enhanced the antibacterial function by generating ROS by AIE moiety under light irradiation. After 30 min of irradiation with white light, TriPE-NT caused death of all *Escherichia coli* (*E. coli*), *Staphylococcus epidermidis*

(*S. epidermidis*), and MDR *S. epidermidis*, and more than 96% death of MDR *E. coli*, *Staphylococcus aureus* (*S. aureus*), and MDR *S. aureus*. We systematically investigated the bacterial killing mechanism of TriPE-NT by characterizing the integrity of the bacterial membrane and TriPE-NT distribution in bacteria by taking advantage of fluorescence emitted by the aggregated TriPE-NT in bacteria. As an example of application, TriPE-NT successfully cured wounds infected by *E. coli*, MDR *E. coli*, *S. epidermidis*, and MDR *S. epidermidis* on rats with negligible inflammatory reaction. Collectively, TriPE-NT showed its advantage of multiple-functions including imaging, monitoring, and bacterial infection inhibition in this study and has great potential for integrated diagnosis and treatment in clinical practices.

2. Results and Discussion

2.1. Synthesis and Characterization of TriPE-NT

The synthetic route for TriPE-NT is shown in **Scheme 1**. Compound 4,4'-dimethoxytriphenylethylene-4,4,5,5-tetramethyl-1,3,2-dioxaborolane (**3**) and 4-bromo butyl-naphthalimide were synthesized according to the reported method in literature.^[23,25] Suzuki coupling of **3** and 4-bromobutyl naphthalimide yielded compound **2** in a moderate yield. The S_N2 reaction between compound **2** and triazole yielded compound **1** efficiently. Finally, TriPE-NT was readily prepared by S_N2 reaction between compound **1** and 1-(bromomethyl)-2,4-difluorobenzene in a yield of 52% (Scheme 1). TriPE-NT and all the intermediate products were fully characterized by nuclear magnetic resonance spectroscopy (¹H NMR, ¹³C NMR) and high-resolution mass spectroscopy (HRMS) with satisfactory results (Figures S1–S9, Supporting Information). We also obtained the single crystal of intermediate **2** which further confirmed the structure of TriPE-NT (Figure S10, Supporting Information).

The optical properties of TriPE-NT were investigated by UV–vis and photoluminescence (PL) spectra. TriPE-NT exhibited two absorption peaks at 324 and 385 nm, which should be ascribed to the π–π* transition and intramolecular charge transfer (ICT) absorption from the TriPE moiety to the naphthalene diimides

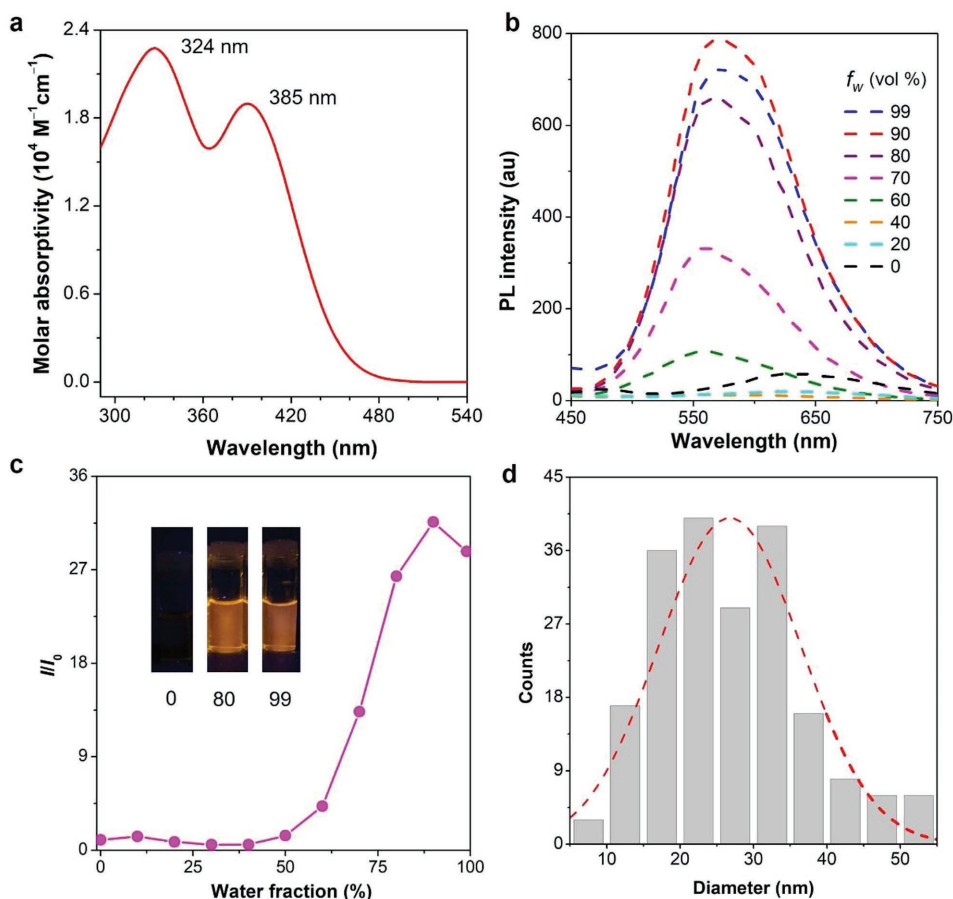


Figure 1. The characterization of TriPE-NT. a) UV-vis absorption spectrum of the aqueous solution of TriPE-NT. b) PL spectra of TriPE-NT in THF/water mixtures with different water fractions (f_w). Concentration: 10×10^{-6} M, excitation wavelength: 385 nm. c) Plotting of PL intensity versus the composition of the THF/water mixture for dissolving TriPE-NT. Inset: photographs of TriPE-NT in THF/water mixtures with water fraction of 0%, 80%, and 99% under 365 nm UV irradiation. d) Size distribution of the TriPE-NT aggregates calculated from FE-SEM data.

segment.^[26] The molar absorptivity of the wavelength at 385 nm was as high as 20 000 (Figure 1a), demonstrating its good conjugation and strong absorption. TriPE-NT is nonemissive in tetrahydrofuran (THF) but brightly emissive in solid state, we thus investigated its AIE characteristic by adding water to its THF solution. With the water fraction increasing from 0% to 60%, TriPE-NT showed a low PL intensity but a long emission wavelength at about 630 nm. However, when the water fraction rose to above 60%, the PL intensity of TriPE-NT intensified significantly and reached the maximum value at a water fraction of 90%, with the emission wavelength blue-shifting to about 570 nm, suggesting that TriPE-NT is a typical AIEgen with twisted ICT (TICT) characteristic (Figure 1b).^[27] The plotting of relative PL intensity (I/I_0) of TriPE-NT at different water fractions demonstrated its AIE activity (Figure 1c). The aggregation behavior of TriPE-NT was characterized by field emission scanning electron microscope (FE-SEM) (Figure S11, Supporting Information). The nanoaggregates of the TriPE-NT showed good homogeneity at a concentration of 10×10^{-6} M (Figure 1d; Figure S11, Supporting Information). Under FE-SEM, the nanoaggregates showed excellent dispersity and a size of ≈ 15 –40 nm (Figure 1d), which further corroborated the aggregates formation of TriPE-NT (Figure S12, Supporting Information). To gain

more insights into the photophysical properties of TriPE-NT, we carried out molecular simulation at the DFT B3LYP/6-31G* level with the Gaussian 09 package. The electron density distribution of the highest occupied molecular orbitals were mainly delocalized over the TriPE part of the molecules, whereas that of the lowest unoccupied molecular orbitals were localized on the naphthalimide groups, which undoubtedly demonstrated the TICT effect (Figure S13, Supporting Information).

2.2. TriPE-NT Sensitized ROS Generation

Traditional PSs such as porphyrin usually show reduced ROS generation in the aggregated state due to the π - π stacking increased nonradiative decay, which can greatly quench the lowest singlet state (S_1). In this context, AIEgens as PSs can offer high ROS production efficiency in aggregated state, since the twisted structure of AIEgens can effectively avoid the π - π stacking-caused S_1 quenching.^[28–31] On the other hand, AIEgens with TICT characteristic have been demonstrated to facilitate effective 1O_2 producing.^[9,32] We subsequently tested ROS generation by using dichlorofluorescein (DCFH), a commercially available ROS indicator. The fluorescence

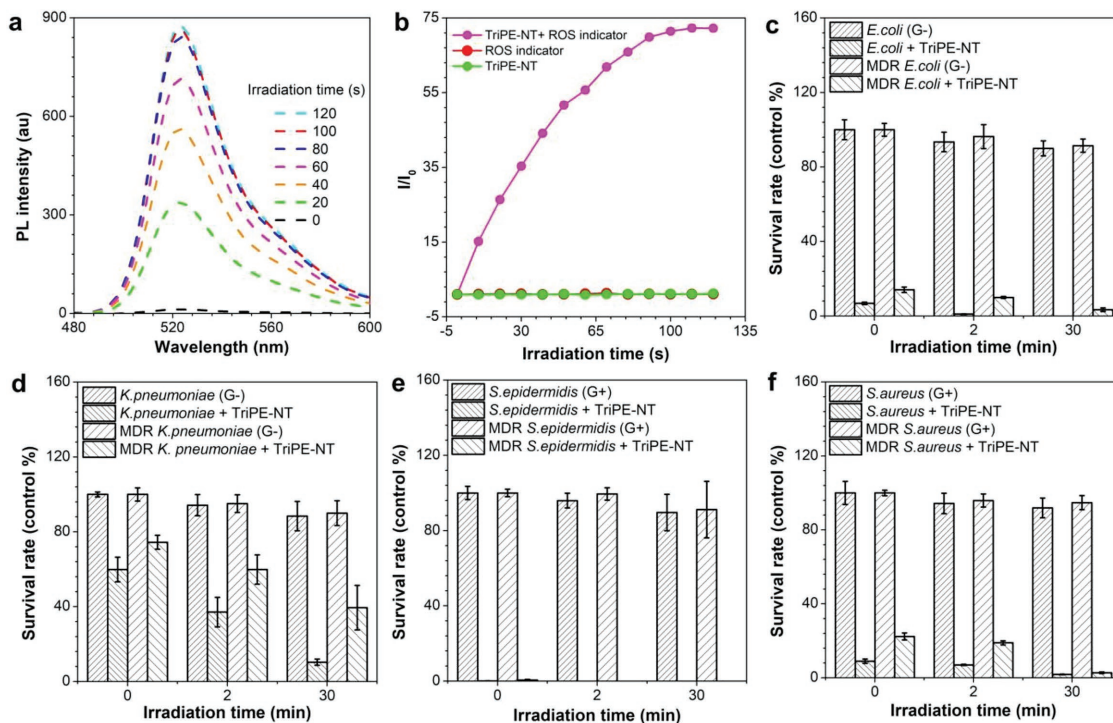


Figure 2. Light-induced ROS generation of TriPE-NT and bacteria inhibition. a) PL spectra of DCFH indicate the generation of ROS by TriPE-NT (10×10^{-6} M) after white light irradiation (4 mW cm^{-2}) for different time periods. Excitation wavelength: 385 nm. b) Plotting of relative PL intensity (I/I_0) at 385 nm versus the irradiation time. Bacteria survival rates of c) *E. coli* and MDR *E. coli*, d) *K. pneumoniae* and MDR *K. pneumoniae*, e) *S. epidermidis* and MDR *S. epidermidis*, and f) *S. aureus* and MDR *S. aureus* are illustrated. The bacteria were incubated with TriPE-NT (10×10^{-6} M) for 10 min, the bacteria suspensions ($50 \mu\text{L}$) were plated on agar plates and treated by white-light illumination (4 mW cm^{-2}) for 0, 2, and 30 min, respectively. Bacteria without TriPE-NT treatment or without light illumination were used as control groups. The data show significant statistical differences between the bacteria groups with or without TriPE-NT treatment.

of DCFH will be lit-up if it is in the presence of ROS species. As shown in **Figure 2a**, under white light irradiation, DCFH showed negligible emission in the visible region. However, in the presence of both DCFH and TriPE-NT with white light irradiation, DCFH exhibited gradually increased fluorescence at around 530 nm (Figure 2b), demonstrating that TriPE-NT as a photosensitizer can generate ROS under white light irradiation.

2.3. Light-Enhanced Bacteria Killing

We evaluated the bacteria killing effect of TriPE-NT on both wild and clinically isolated MDR bacteria by a traditional plate counting method.^[5] First, *E. coli* and *S. epidermidis*, as the representative of Gram-negative (G⁻) and Gram-positive (G⁺) bacteria, were used to determine the effective bactericidal concentration and illumination time. The bacteria were incubated with TriPE-NT (0, 5, 10×10^{-6} M) for 0 and 10 min, the bacteria suspensions ($50 \mu\text{L}$) were plated on agar plates and treated by white-light illumination (4 mW cm^{-2}) for 2, 10, and 30 min, respectively (Figure S14, Supporting Information). TriPE-NT at a concentration of 10×10^{-6} M ($8.4 \mu\text{g mL}^{-1}$) killed all *E. coli* after white light irradiation of 30 min, while all *S. epidermidis* were killed by a lower TriPE-NT concentration (5×10^{-6} M,

$4.2 \mu\text{g mL}^{-1}$) after light irradiation of 2 min. The possible reason for this difference may be ascribed to the extra membrane of G⁻ bacteria which is absent in G⁺ bacteria.^[33,34] Also, according to the preliminary experiments, 10×10^{-6} M TriPE-NT and light irradiation for 2 or 30 min were set as experimental conditions in the following experiments.

As for G⁻ bacteria *E. coli*, MDR *E. coli*, *Klebsiella pneumoniae* (*K. pneumoniae*), MDR *K. pneumoniae*, and G⁺ bacteria *S. epidermidis*, MDR *S. epidermidis*, *S. aureus*, and MDR *S. aureus*, colony counting showed that TriPE-NT had potent light-enhanced antibacterial activity (Figure S15, Supporting Information). In darkness, 10×10^{-6} M ($8.4 \mu\text{g mL}^{-1}$) TriPE-NT killed nearly all MDR *S. epidermidis* (Figure 2e, 0 min), while the survival rates of *E. coli*, MDR *E. coli*, *K. pneumoniae*, MDR *K. pneumoniae*, *S. aureus*, and MDR *S. aureus* were $\approx 6.8\% \pm 0.6\%$, $14.1\% \pm 1.4\%$, $59.9\% \pm 6.5\%$, $74.4\% \pm 3.7\%$, $8.9\% \pm 1.1\%$, and $22.4\% \pm 1.9\%$, respectively (Figure 2c,d,f). Therefore, TriPE-NT itself can work as a superior antibiotic. Under irradiation with white light (4 mW cm^{-2} , 30 min), all *E. coli* and more than 96% MDR *E. coli*, 90% *K. pneumoniae*, 61% MDR *K. pneumoniae*, 98% *S. aureus*, and 97% MDR *S. aureus* were killed (Figure 2c,d,f), indicating light irradiation can further promote the antibacterial activity of TriPE-NT even for MDR bacteria. TriPE-NT agents plus light irradiation were more effective to inhibit *S. epidermidis* or MDR *S. epidermidis* than *E. coli*, MDR *E. coli*, *K. pneumoniae* or MDR

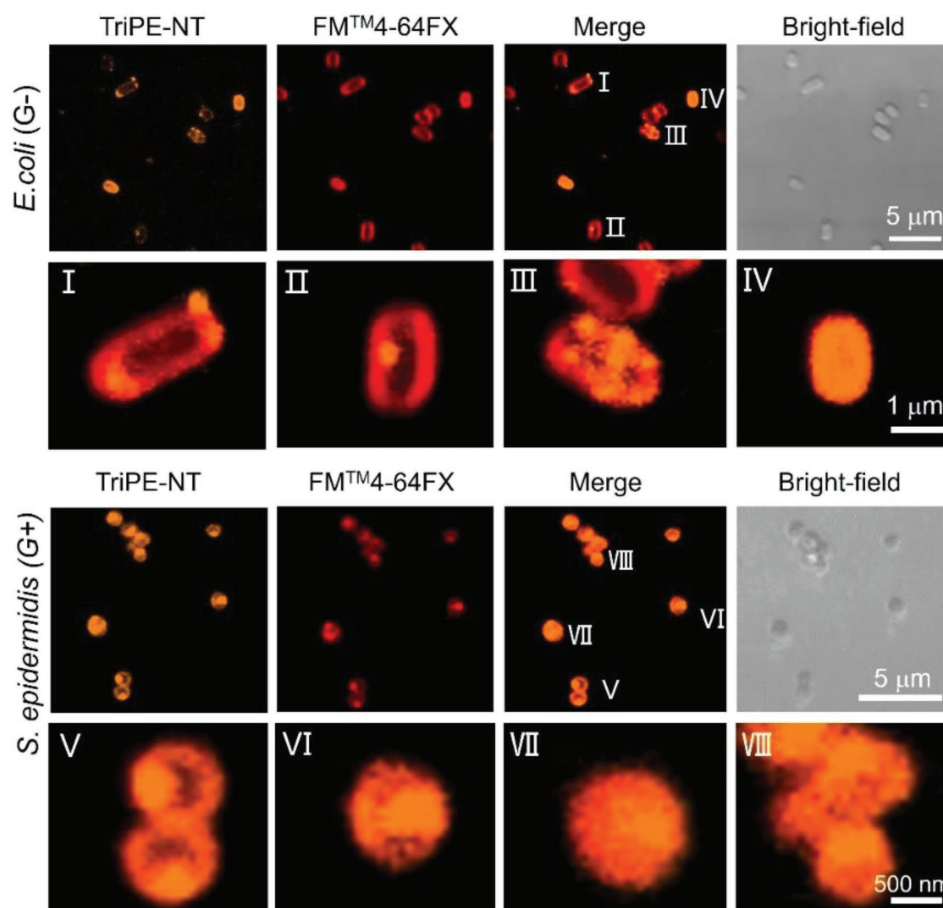


Figure 3. Bright-field and fluorescent images of bacteria. *E. coli* (G⁻) and *S. epidermidis* (G⁺) were incubated with 10×10^{-6} M of TriPE-NT (orange) and FM4-64FX (red) for 10 min before imaging. TriPE-NT: Ex, 405 nm, Em, 500–560 nm; FM4-64FX: Ex, 543 nm, Em, 600–700 nm.

K. pneumoniae (Figure S16, Supporting Information). Also, *S. aureus* and MDR *S. aureus* were susceptible to TriPE-NT plus light irradiation than *K. pneumoniae* or MDR *K. pneumoniae* (Figure S16, Supporting Information). By comparison, polymyxin, the last line treatment for MDR G⁻ bacterial infections, showed antibacterial activity to MDR *E. coli* and MDR *K. pneumoniae*, at a minimum inhibition concentration surpassing 32 or 64 $\mu\text{g mL}^{-1}$, respectively (Table S1, Supporting Information).^[35,36] By contrast, TriPE-NT effectively inhibited not only G⁻ bacteria but also G⁺ bacteria at a relatively low concentration, demonstrating its superior antibacterial activities over conventional antibiotics.

We tested cytotoxicity of the TriPE-NT because a good antibacterial drug should have the ability to kill only bacteria but have no toxicity to human or animal cells. The biocompatibility of TriPE-NT was evaluated by CCK-8 kit. The cell viabilities of human skin fibroblast cells (HAFs) and human umbilical vein endothelial cells (HUVECs) were not significantly changed with the increasing concentration of TriPE-NT (2, 5, 10, and 20 $\times 10^{-6}$ M) in the absence of white light irradiation (4 mW cm^{-2}), and no obvious cytotoxicity was observed with the increase of irradiation time (Figure S17, Supporting Information), demonstrating the high safety of TriPE-NT for mammalian cells.

2.4. Preliminary Mechanistic Studies

2.4.1. Bacteria Staining and Imaging

To understand how TriPE-NT works, we stained the bacteria by TriPE-NT. The pure solution of *E. coli* (G⁻) or *S. epidermidis* (G⁺) showed weak blue color under 365 nm UV irradiation, while the pure TriPE-NT (10×10^{-6} M) was orange under the same irradiation. After incubation with 10×10^{-6} M TriPE-NT for 10 min, the solution containing *E. coli* or *S. epidermidis* emitted strong yellow fluorescence under 365 nm UV irradiation (Figure S18, Supporting Information).

To directly observe the interactions between TriPE-NT and the bacteria, we coincubated bacteria with TriPE-NT and FM4-64FX (a lipid membrane dye) and conducted fluorescence imaging using confocal laser scanning microscopy (CLSM). For most of the *E. coli*, TriPE-NT only stained the cell membrane (Figure 3, I–IV). By contrast, for *S. epidermidis*, the probe lit up almost the whole bacteria, including the membrane and the cytosol (Figure 3, V–VIII). This phenomenon implies that it may be easier for TriPE-NT to penetrate into *S. epidermidis* than into *E. coli*, as the latter contains an extra outer membrane.^[33,34]

To indicate the status of the bacteria after TriPE-NT treatment, we incubated the bacteria with commercial dead

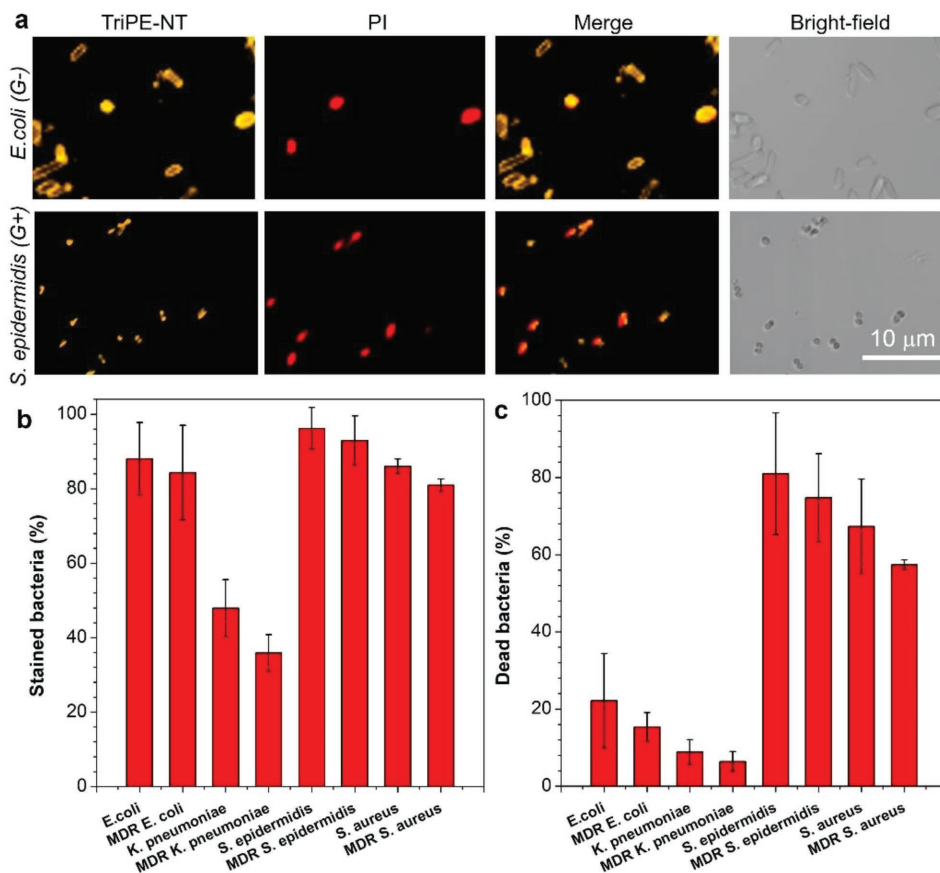


Figure 4. Bacterial staining and statistical analysis. a) Bright-field and fluorescent images of *E. coli* and *S. epidermidis* incubated with 10×10^{-6} M of TriPE-NT (orange) and propidium iodide (PI) (red) for 10 min. TriPE-NT: Ex, 405 nm, Em, 500–560 nm; PI: Ex, 514 nm, Em, 600–700 nm. Statistical data of b) TriPE-NT-stained bacteria and c) dead bacteria stained by PI were obtained by counting the number of stained bacteria after the bacteria were incubated with 10×10^{-6} M of TriPE-NT or PI for 10 min.

bacteria-staining fluorescent reagent propidium iodide (PI) and TriPE-NT at the same time. Thanks to the AIE characteristics and water solubility of TriPE-NT, there was almost no background fluorescence in the imaging field. *E. coli* and *S. epidermidis*, which emitted bright orange (TriPE-NT) or red (PI) fluorescence, are clearly visualized under CLSM (Figure 4a; Figures S19–20, Supporting Information). We found that TriPE-NT can stain almost all the G+ bacteria (e.g., $96.2\% \pm 5.6\%$ *S. epidermidis*, $92.9\% \pm 6.6\%$ MDR *S. epidermidis*, $86.1\% \pm 1.9\%$ *S. aureus*, and $80.9\% \pm 1.7\%$ MDR *S. aureus*) (Figure 4b; Figure S20, Supporting Information), no matter they were alive or dead (red). In comparison, relatively low percentage of G– bacteria were stained by TriPE-NT (e.g., $88.1\% \pm 9.8\%$ *E. coli*, $84.3\% \pm 12.7\%$ MDR *E. coli*, $47.9\% \pm 7.7\%$ *K. pneumoniae* and $35.8\% \pm 4.9\%$ MDR *K. pneumoniae*) (Figure 4b; Figure S19, Supporting Information). Notably, almost all the *S. epidermidis* ($80.9\% \pm 15.8\%$ *S. epidermidis*) were costained by TriPE-NT and PI (Figure 4a,c), this is similar to other G+ bacteria ($74.8\% \pm 11.4\%$, MDR *S. epidermidis*, $67.3\% \pm 12.2\%$, *S. aureus*, and $57.4\% \pm 1.3\%$, MDR *S. aureus*) (Figure 4a,c; Figure S20, Supporting Information). By contrast, relatively low percentage of *E. coli* ($22.1\% \pm 12.2\%$) were costained by both TriPE-NT and PI (Figure 4a,c), which is also similar to other G– bacteria ($15.3\% \pm 3.7\%$, MDR *E. coli*, $8.8\% \pm 3.2\%$, *K. pneumoniae*, and $6.4\% \pm$

2.6% MDR *K. pneumoniae*) (Figure 4a,c; Figure S19, Supporting Information). The reason for this difference possibly is ascribed to the extra membrane of G– bacteria which is absent in G+ bacteria.^[33,34] These observations also illustrated that both G– bacteria and G+ bacteria are vulnerable to TriPE-NT treatment, the possible reason is that these bacteria with negatively charged membranes (Figure S21a, Supporting Information), could anchor, uptake, and aggregate the positively charged probe (Figure S21b, Supporting Information), which restricts the intramolecular motion of the probe and causes their fluorescence emission.^[11]

2.4.2. FE-SEM and Field-emission High Resolution Transmission Electron Microscope (FEHR-TEM) Characterizations

To gain more insights into the TriPE-NT–bacteria interactions, we employed FE-SEM and FEHR-TEM to visualize the morphological changes of the bacteria under TriPE-NT treatment, selecting *E. coli* (G–), MDR *E. coli* (G–), and *S. epidermidis* (G+), MDR *S. epidermidis* (G+) as representatives. Without TriPE-NT treatment, the four kinds of bacteria showed regular shape with clear borders and cell walls (Figure 5a). *E. coli* or MDR *E. coli* treated by TriPE-NT in the absence of white

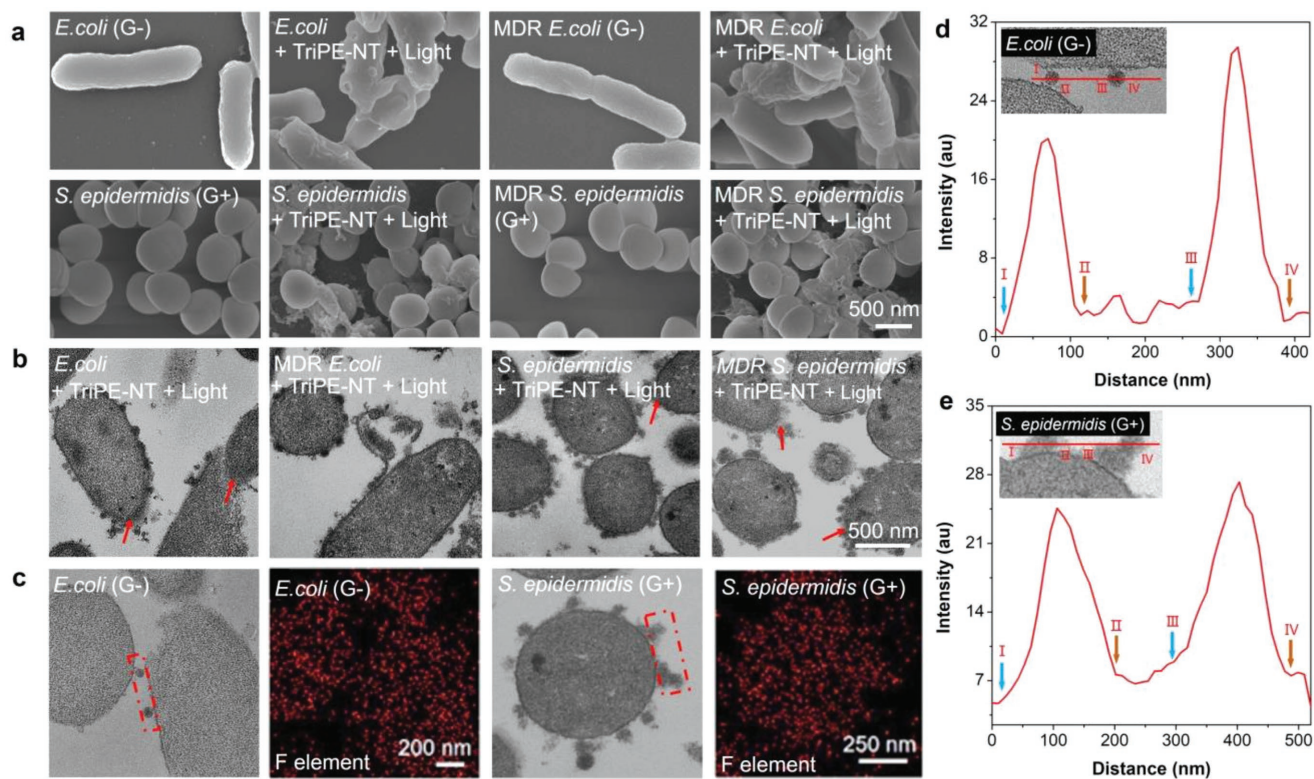


Figure 5. Visualizing TriPE-NT-induced morphological changes of bacteria. *E. coli*, MDR *E. coli*, *S. epidermidis*, and MDR *S. epidermidis* with white light irradiation were imaged by FE-SEM and FEHR-TEM, bacteria without treatment were set as controls. a) FE-SEM images. b) FEHR-TEM images, the red arrows indicate the destroyed membrane. c) Elemental mapping of F (red color) of *E. coli* and *S. epidermidis*. d) The elemental curve measured on the superthin slices of TriPE-NT-treated *E. coli* (from the region marked by red rectangle in (c)). e) The elemental curve measured on the superthin slices of TriPE-NT-treated *S. epidermidis* (from the region marked by red rectangle in (c)).

light showed obvious rough surface and damaged cell wall (Figure S22, Supporting Information), and light irradiation further exacerbated the damage where cell wall fragmentations can be observed (Figure 5a). For *S. epidermidis* and MDR *S. epidermidis*, TriPE-NT treatment without or with light irradiation (4 mW cm^{-2} , 30 min) led to wrinkled bacterial cell wall (Figure 5a; Figure S22, Supporting Information). Parts of TriPE-NT-treated bacteria showed broken cell walls (red arrow) and many granular substances on the surface of the bacteria (Figure 5b).

2.4.3. Elemental Scan Analysis

We used elemental scan analysis on bacterial superthin slices (60–70 nm in thickness) to verify if TriPE-NT can enter bacterial cells. Bacteria are usually composed of elements including carbon (C), nitrogen (N), and oxygen (O), while TriPE-NT molecule is composed of C, N, O, and fluorine (F) elements. In this study, we analyzed the distribution of F elements in the TriPE-NT-treated *E. coli* and *S. epidermidis*. The imaging (Figure 5c) and signal analysis (Figure 5d,e) demonstrated that both *E. coli* and *S. epidermidis* showed the signals of F element which was contributed by TriPE-NT. The results indicate that TriPE-NT can attach on the cell wall or enter into the bacteria.

2.5. Evaluation on Rat Wound Models

To further evaluate the anti-bacterial activity of TriPE-NT in vivo, we tested the performance of TriPE-NT on bacteria-infected wounds of rats. We established *E. coli*-, MDR *E. coli*-, *S. epidermidis* or MDR *S. epidermidis*-infected, full-thickness skin wounds on the dorsal skin of the Wistar rats (Figure 6a; Figure S23, Supporting Information). We captured the macroscopic appearance of the healing processes of the wounds at different time points (Figure 6b). On day 3 postinjury, all the wounds showed no apparent difference (Figure 6c). On day 7, the sizes of the MDR *E. coli*-infected wounds treated by TriPE-NT plus light irradiation (4 mW cm^{-2} , 30 min) were significantly smaller than those of the control groups respectively, while *E. coli*-infected wounds treated by TriPE-NT agents plus light had more apparent reduction of wound size on day 7 postinjury (Figure 6c). MDR *S. epidermidis*-infected wounds treated by TriPE-NT agents plus light irradiation (4 mW cm^{-2} , 30 min) showed significantly smaller sizes than the control groups on day 7 postinjury, while the *S. epidermidis*-infected wounds treated by TriPE-NT agents plus light irradiation showed more apparent reduction of wound size on day 7 postinjury (Figure 6d). By comparison, under the same TriPE-NT plus light irradiation, *S. epidermidis* or MDR *S. epidermidis*-infected wounds showed faster healing rate than *E. coli* or MDR *E. coli*-infected wounds (Figure S24, Supporting Information).

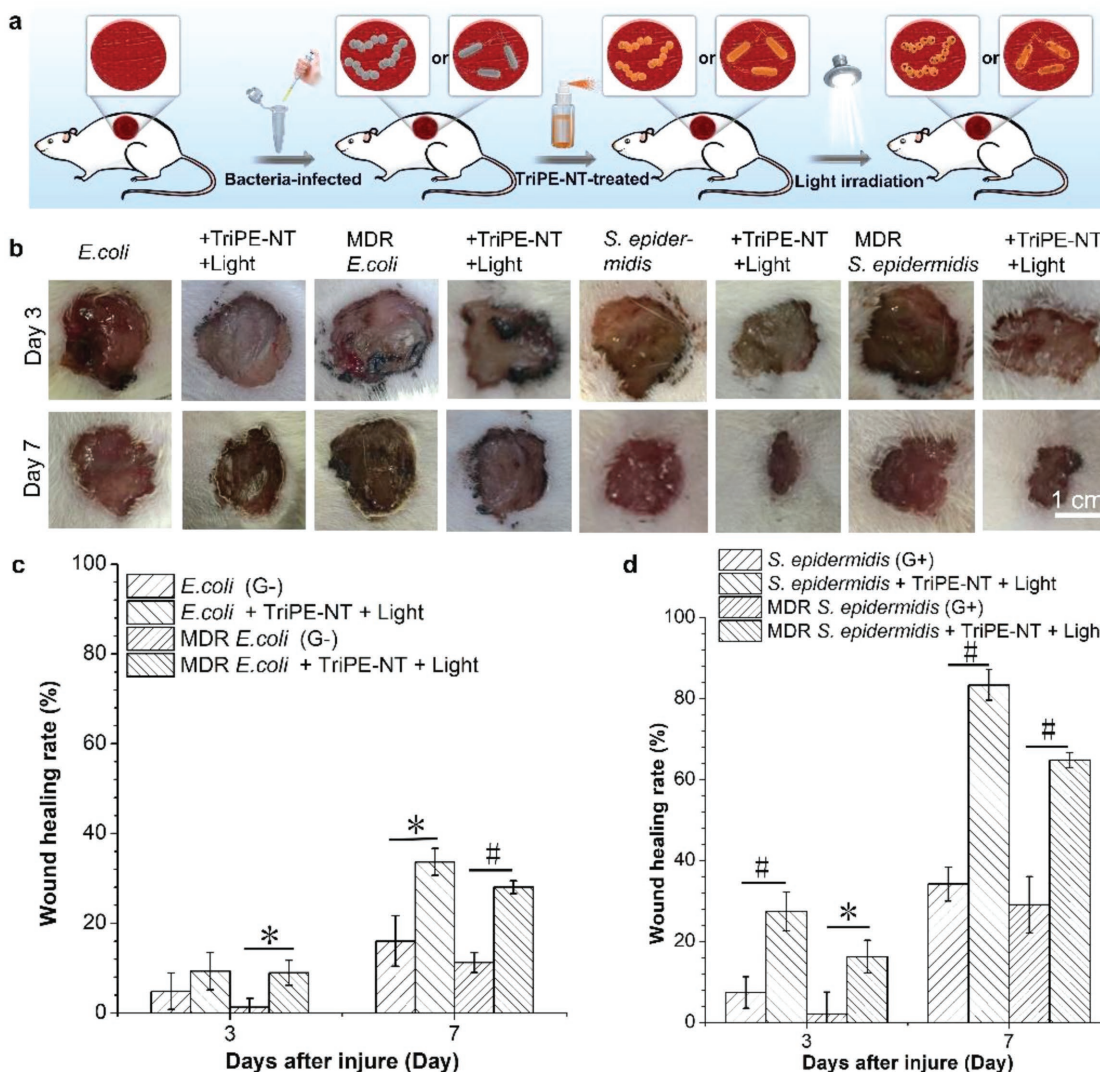


Figure 6. In vivo evaluation of TriPE-NT in treatment of bacteria-infected wounds on rats. a) The cartoon illustrates the process of establishing bacteria-infected full-thickness skin wound models on rats. b) Photographs of wounds treated by TriPE-NT plus white-light irradiation (4 mW cm^{-2}) after injury for different time periods. c) The proportion of the *E. coli*- and MDR *E. coli*-infected wound area on day 3, day 7 after the injury. d) The proportion of the *S. epidermidis*- and MDR *S. epidermidis*-infected wound area on day 3, day 7 after the injury ($n = 5$). The data show significant statistical differences between bacteria-infected groups and bacteria-infected wounds treated by TriPE-NT plus light irradiation ($0.001 < *P < 0.05$, $\#P < 0.001$).

The result agrees with the in vitro testing that TriPE-NT agents plus light irradiation were more effective to inhibit *S. epidermidis* or MDR *S. epidermidis* than *E. coli* or MDR *E. coli* (Figure 2; Figure S15, Supporting Information).

We carried out hematoxylin and eosin (HE) staining for evaluating the wound healing of the sectioned tissues of the *E. coli*-, MDR *E. coli*-, *S. epidermidis*-, and MDR *S. epidermidis*-infected wounds on the Wistar rats on day 3 and day 7 postinjury (Figure 7). On day 3 postinjury, the *E. coli*-, MDR *E. coli*-, *S. epidermidis*-, and MDR *S. epidermidis*-infected wounds without TriPE-NT plus light irradiation treatment showed more invaded lymphocytes than the samples treated by TriPE-NT plus light irradiation, implying that TriPE-NT plus light irradiation successfully reduced the inflammatory reactions. On day 7 postinjury, *S. epidermidis*- or MDR *S. epidermidis*-infected wounds treated by TriPE-NT plus light irradiation displayed

the appearance of fibroblasts and newly formed squamous epithelial layers, which can hardly be seen in the control groups. Fibroblasts can secrete collagens which accelerate wound reconstruction,^[37] that means the TriPE-NT plus light irradiation can promote the wound healing. On day 7 postinjury, the bacteria-infected wounds treated by TriPE-NT plus light irradiation showed appearance of hair follicles in *S. epidermidis*-infected wounds. The in vivo experiments demonstrated that the TriPE-NT plus light irradiation had successfully suppressed the bacterial infections and promoted the wound healing.

3. Conclusion

In summary, we developed a bifunctional AIE luminogen TriPE-NT by connecting an AIE unit TriPE (fluorescent part)

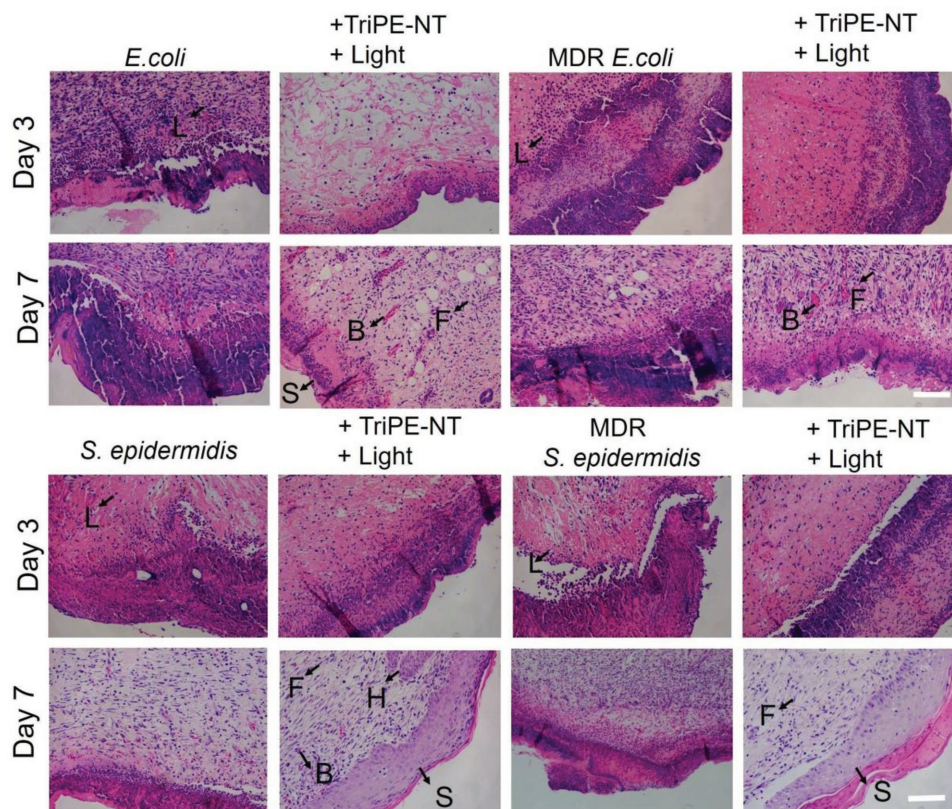


Figure 7. HE staining of the sectioned tissues of wounds on rats. *E. coli*, MDR *E. coli*, *S. epidermidis*- or MDR *S. epidermidis*-infected wounds were treated with or without TriPE-NT plus white-light irradiation. The tissues were resected on day 3 and 7 after injury. The letters in the images indicate specific cell types and structures in the histological sections. L: lymphocytes; B: blood vessels; F: fibroblasts; S, squamous epithelial cell; H, hair follicle. All scale bars equal to 100 μm .

with NT (antibacterial part). TriPE-NT can simultaneously stain and kill bacteria in darkness. Furthermore, under ordinary light irradiation, its antibacterial efficacy increases dramatically. TriPE-NT is a broad-spectrum bactericide, which can enter and kill Gram-positive bacteria and Gram-negative bacteria. More importantly, TriPE-NT can kill multidrug-resistant bacteria which are posing immense threat to human health. TriPE-NT, therefore, is promising not only to serve as a potent antibacterial agent, but also as a convenient *in vitro* bacteria detecting agent for clinical applications. This study also provides a new strategy for designing multifunctional antibiotics for a wider spectrum of applications.

4. Experimental Section

Materials and Characterization: Compound 4 was from AIEgen Biotech Co., Ltd. All other chemicals and solvents were from Sigma-Aldrich or Acros. THF was dried by distillation using sodium as drying agent and benzophenone as an indicator. Luria-Bertani (LB) broth and LB agar were from USB Co. Zinc dust, Phosphate buffer saline (PBS) was from Sigma-Aldrich. PI was from DojinDo. *E. coli*, *K. pneumoniae*, *S. epidermidis*, and *S. aureus* were from ATCC. MDR *E. coli*, MDR *K. pneumoniae*, MDR *S. epidermidis*, and MDR *S. aureus* were from Beijing Tiantan Hospital (China), Milli-Q water was from a Milli-Q purification system (Merck Millipore, Germany). NMR

spectra were measured on a Bruker ARX 400 NMR spectrometer using tetramethylsilane (TMS; $\delta = 0$) as internal reference. HRMS was obtained on a Finnigan MAT TSQ 7000 Mass Spectrometer System operated in a MALDI-TOF mode. UV-vis spectra were measured on a Milton Roy Spectronic 3000 Array spectrophotometer. Dynamic light scattering was performed on a ZetaPlus (Brookhaven Instruments Corporation). Steady-state PL spectra were measured on a Perkin-Elmer spectrofluorometer LS 55.

Synthesis: 4,4'-dimethoxytriphenylethylene-4,4,5,5-tetramethyl-1,3,2-dioxaborolane (compound) 3 and 6-bromo-2-(4-bromobutyl)-naphthalenediimide was synthesized according to the literature method.^[22,38] Synthesis of compound 2. Compound 3 (210 mg, 0.47 mmol), 6-bromo-2-(4-bromobutyl)-naphthalenediimide (150 mg, 0.36 mmol), Pd(PPh₃)₄ (116 mg, 28%), and K₂CO₃ (497 mg, 3.6 mmol) were dissolved in the mixture of distilled THF (15 mL) and deoxygenated H₂O (6 mL) under nitrogen. The mixture was then stirred at 80 °C for 48 h. After cooling to room temperature, the mixture was washed with water twice and extracted with dichloromethane. After solvent evaporation, the crude product was purified by silica-gel chromatography using chloroform as eluent and recrystallization, affording 140 mg of 2. Yield: 60%. ¹H NMR (400 MHz, CDCl₃, 25 °C), δ (ppm): 8.61–8.58 (m, 2H), 8.30–8.28 (d, *J* = 8 Hz, 1H), 7.70–7.65 (m, 2H), 7.32–7.28 (m, 4H), 7.23–7.19 (m, 4H), 6.94–6.87 (m, 5H) 4.25–4.22 (m, 2H), 3.86 (s, 3H), 3.83 (s, 3H), 3.50–3.47 (m, 3H), 2.03–1.91 (m, 4H). ¹³C NMR (100 MHz, CDCl₃, 25 °C), δ (ppm): 163.7, 163.5, 158.8, 158.5, 146.2, 142.4, 137.7, 135.8, 135.5, 132.2, 131.9, 130.9, 130.6, 130.3, 129.2, 129.0, 128.3, 128.1, 127.1, 126.1, 124.5, 122.1, 120.7, 113.6, 113.0, 54.6, 50.2, 38.7, 32.6, 29.7, 26.3. HRMS (MALDI-TOF): *m/z*: [M]⁺ calcd for C₃₈H₃₂BrNO₄, 645.1515; found, 645.1544.

Synthesis of Compound 1: Compound 2 (65 mg, 0.1 mmol), 1,2,4-triazole (10 mg, 0.14 mmol), K_2CO_3 (21 mg, 0.15 mmol), and TBAB (5 mg) were dissolved in CH_3CN (5 mL) and stirred at 60 °C under nitrogen. After 1 h, a large amount of yellow pellet was precipitated and collected. The crude product was purified by silica-gel chromatography using DCM/ CH_3OH = 4/1 as eluent, affording 32 mg of 1. Yield: 50%. 1H NMR (400 MHz, $CDCl_3$, 25 °C), δ (ppm): 8.62–8.60 (t, d = 4 Hz, 2H), 8.32–8.30 (d, J = 8 Hz, 1H), 8.16 (s, 1H), 7.94 (s, 1H), 7.72–7.67 (m, 2H), 7.33–7.30 (m, 4H), 7.24–7.20 (m, 4H), 6.94–6.88 (m, 5H) 4.33–4.25 (m, 4H), 3.87 (s, 3H), 3.83 (s, 3H), 3.50–3.47 (m, 3H), 2.05–2.01 (m, 2H), 1.82–1.79 (m, 2H). HRMS (MALDI-TOF): m/z : $[M]^+$ calcd for $C_{40}H_{34}N_4O_4$, 634.2580; found, 634.2538.

Synthesis of Compound TriPE-NT: Compound 1 (63 mg, 0.1 mmol) and 1-(bromomethyl)-2,4-difluorobenzene (31 mg, 0.15 mmol) dissolved in CH_3CN (5 mL) were stirred in CH_3CN at 80 °C under nitrogen for 5 h. The mixture was cooled to room temperature and the solvent was removed under reduced pressure. The crude product was recrystallized with ether and DCM twice, affording 36 mg of 1. Yield: 43%. 1H NMR (400 MHz, $CDCl_3$, 25 °C), δ (ppm): 11.65–11.55 (t, d = 4 Hz, 2H), 8.84–8.73 (m, 1H), 8.51 (br, 2H), 8.25–8.16 (m, 2H), 7.63 (br, 2H), 7.32–7.19 (m, 8H), 6.93–6.88 (m, 7H) 6.00 (s, 2H), 4.65 (s, 2H), 4.22–4.20 (s, 2H), 3.85 (s, 6H), 2.15 (br, 2H), 1.86 (br, 2H). ^{13}C NMR (100 MHz, $CDCl_3$, 25 °C), δ (ppm): 164.3, 164.1, 159.5, 159.2, 146.9, 143.7, 143.1, 138.3, 136.3, 136.1, 132.9, 132.5, 131.5, 131.3, 130.9, 129.8, 129.6, 128.9, 128.6, 127.7, 126.7, 125.1, 122.4, 121.1, 114.1, 113.7, 55.4, 55.3, 52.6, 45.5, 39.1, 31.6, 26.3, 24.6, 22.6. HRMS (MALDI-TOF): m/z : $[M]^+$ calcd for $C_{47}H_{39}F_2N_4O_4$, 761.2934; found, 761.2951.

Sample Preparation: A stock solution of TriPE-NT in DMSO with a concentration of 10×10^{-3} M was prepared and stocked at room temperature. LB broth, LB agar, and PBS medium were prepared according to the protocol on the product description. The medium was sterilized for 20 min at 121 °C before plating the bacteria.

Detection of ROS in Solution: DCFH as an ROS indicator was used to detect the ROS generation in solution under white light irradiation (4 mW cm^{-2}). ROS indicator (40×10^{-6} M) in PBS was prepared according to the reagent supplies user manual and further diluted to 5×10^{-6} M in sample solution (10×10^{-6} M) for measurement by PL instrument. The PL spectra of 2,7-dichlorofluorescein activated by TriPE-NT generated ROS under white light were measured for different time intervals (0, 20, 40, 60, 80, 100, and 120 s). The fluorescence spectra were measured with excitation at 385 nm and emission from 480 to 600 nm.

Antimicrobial Assay: For the light-induced toxicity experiment, 10^8 CFU mL^{-1} bacteria were dispersed in 1 mL of 5 or 10×10^{-6} M TriPE-NT PBS solution. 50 μL (10^5 CFU mL^{-1} bacteria) of the bacteria solution was sprayed onto an LB agar plate, the plate exposed to white light (4 mW cm^{-2}) for designed periods of time (0, 2, 10, and 30 min), while the control groups were put in darkness, and then cultured at 37 °C for 24 h before quantification or imaging.

Bacteria Culturing, Staining, and Imaging: *E. coli*, MDR *E. coli*, *K. pneumoniae*, MDR *K. pneumoniae*, *S. epidermidis*, MDR *S. epidermidis*, *S. aureus*, and MDR *S. aureus* were cultured in the LB medium at 37 °C with a shaking speed of 200 rpm. Bacteria were harvested by centrifuging at 8000 rpm for 3 min and washed twice. The optical density of the bacteria suspension was measured on a microplate reader (Tecan, infinite M200, Switzerland) at 600 nm. 1 mL of TriPE-NT solution in PBS (10×10^{-6} M) and PI (200×10^{-9} M) or FM4-64FX (0.2 mL from a $5 \mu g mL^{-1}$ stock solution in PBS) containing 5×10^8 colony forming unit (CFU mL^{-1}) of bacteria was transferred to a 1.5 mL microcentrifuge tube. After dispersion with vortex, the bacteria were incubated at 37 °C with a shaking speed of 200 rpm for 10 min. To take fluorescence images, 2 μL of stained bacteria solution was transferred to a piece of glass slide and then covered by a coverslip. The images were collected using a confocal laser scanning microscope (LSM710, Carl Zeiss, Germany).

Preparation of Bacteria Samples for FE-SEM and FEHR-TEM: 200 μL (1×10^4 CFU mL^{-1}) of bacteria suspension was pipetted to 24-well plates after the sterilized cell culture slides were put into the orifice. The bacteria were cultured overnight at 30 °C and then washed twice by PBS before the addition of TriPE-NT PBS (10×10^{-6} M) solution. TriPE-NT-treated

bacteria were cultured at 30 °C for 10 min and then exposed to white light for 30 min. TriPE-NT-treated bacteria samples were fixed with 2.5% glutaraldehyde and dehydrated by 30%, 50%, 70%, 80%, 90%, 95%, and 100% (v/v, in water) ethanol for analysis by FE-SEM (S4800, Hitachi). 5×10^8 CFU mL^{-1} bacteria were dispersed in 1 mL of 10×10^{-6} M TriPE-NT PBS solution in 1.5 mL microcentrifuge tube. The TriPE-NT-treated bacteria solution was incubated at 37 °C with a shaking speed of 200 rpm for 10 min and then exposed to white light for 30 min. The TriPE-NT-treated bacteria were harvested by centrifuging at 8000 rpm for 3 min and fixed by 2.5% glutaraldehyde. The TriPE-NT-treated bacteria samples for TEM characterization were prepared according to the previous reported procedure.^[39] The TriPE-NT-treated bacteria were characterized by FEHR-TEM (JEM-2100F).

Cell Viability Assay: HAFs and HUVECs were cultured in DMEM medium, which contained 10% FBS, 1% penicillin G (P) (100 U mL^{-1}), and streptomycin (S) (100 U mL^{-1}). HAFs and HUVECs were seeded in 96-well plates (1×10^4 cells $200 \mu L^{-1}$) and incubated for 24 h. The medium was removed and TriPE-NT was added at different concentrations and incubated in darkness for 30 min at 37 °C. The TriPE-NT-treated cells were exposed to white light for 2 and 30 min, respectively, and the TriPE-NT-treated cells in darkness were set as control. The cell medium was replaced by fresh medium and incubated for 24 h at 37 °C after irradiation. 100 μL of fresh medium containing 10 μL CCK-8 solution was added into each well after the removal of the cell medium, and the cells were incubated at 37 °C for 2 h. The absorption of the samples was measured on a microplate reader (Tecan, infinite M200, Switzerland) at 450 nm. The results were analyzed by Origin Pro 8.0.

Animal Surgery and Histological Analysis: Normal 8–10 week-old male Wistar rats with an average weight of 350 g (Beijing Vital River Laboratory Animal Technology Co. Ltd., China) were used in the in vivo experiments. All procedures involving animal use were approved by the Institutional Animal Ethical Committee, at Tsinghua Laboratory Animal Research Center (China).

The Wistar rats were randomly divided into 8 groups on the basis of the bacteria-infected skin wounds. The rats were anaesthetized by injection of chloral hydrate 3.5% (10 mL kg^{-1}) in the abdominal cavity. Two full-thickness skin injuries on each rat were prepared by removing a 2.0 cm diameter circular patch of dorsal flank skin on the rat. Bacteria suspension ($100 \mu L$, 1×10^9 CFU mL^{-1}) was added on the surface of the wounds, and the bacteria suspension were kept in the wound for 40 min and TriPE-NT/NaCl solution was (10×10^{-6} M) sprayed on the bacteria-infected wounds (twice, interval 30 min), after treating the wounds by bacteria suspension for 30 min, white-light irradiation (4 mW cm^{-2}) was performed above the wounds for 30 min (with/without TriPE-NT). The rats were fed in separated cages to facilitate the healing of the wounds after the operation. The wound regions were imaged by camera 3 and 7 days postoperation.

Histological analysis of the wounds was carried out on day 3 and day 7 postoperation. The wound tissues were collected and fixed in 4% formaldehyde solution for 30 min. The pathological sections of wound tissues were analyzed by HE staining. Histological images were taken using an inverted microscope (Olympus, IX71, Japan).

Statistical Analysis: The values reported are expressed as mean SD. The Origin 8 software was used for graph plotting. A value of $P < 0.05$ was considered significant. Each experiment included at least three replicates.

Supporting Information

Supporting Information is available from the Wiley Online Library or from the author.

Acknowledgements

Y.L. and Z.Z. contributed equally to this work. This work was in part supported by the Innovation and Technology Commission (ITC-CNRC14SC01),

the Research Grants Council of Hong Kong (16301614, 16305015, 16308016, N-HKUST604/14, and A-HKUST605/16), National Natural Science Foundation of China (21761142006, 31470911, and 81673039), and the Chinese Academy of Sciences (XDA09030305).

Conflict of Interest

The authors declare no conflict of interest.

Keywords

AlEgen, antimicrobial agents, bacterial infections, reactive oxygen species

Received: July 6, 2018

Revised: August 5, 2018

Published online: August 30, 2018

- [1] M. A. Fischbach, C. T. Walsh, *Science* **2009**, 325, 1089.
- [2] S. B. Levy, B. Marshall, *Nat. Med.* **2004**, 10, S122.
- [3] S. J. Lam, N. M. O'Brien-Simpson, N. Pantarat, A. Sulistio, E. H. H. Wong, Y. Y. Chen, J. C. Lenzo, J. A. Holden, A. Blencowe, E. C. Reynolds, G. G. Qiao, *Nat. Microbiol.* **2016**, 1, 16162.
- [4] Y. Li, Y. Tian, W. S. Zheng, Y. Feng, R. Huang, J. X. Shao, R. B. Tang, P. Wang, Y. X. Jia, W. F. Zheng, G. Yang, X. Y. Jiang, *Small* **2017**, 13, 1700130.
- [5] C. F. Xing, Q. L. Xu, H. W. Tang, L. B. Liu, S. Wang, *J. Am. Chem. Soc.* **2009**, 131, 13117.
- [6] C. A. Strassert, M. O. Dipl.-Chem, R. Q. Albuquerque, A. H. Dipl.-Chem, Y. Vida, B. Maier, L. D. Cola, *Angew. Chem., Int. Ed.* **2009**, 48, 7928.
- [7] S. Y. Park, H. J. Baik, Y. T. Oh, K. T. Oh, Y. S. Youn, E. S. Lee, *Angew. Chem., Int. Ed.* **2011**, 50, 1644.
- [8] T. Y. Ohulchanskyy, D. J. Donnelly, M. R. Detty, P. N. Prasad, *J. Phys. Chem.* **2004**, 108, 8668.
- [9] W. B. Wu, D. Mao, F. Hu, S. D. Xu, C. Chen, C. J. Zhang, X. M. Cheng, Y. Y. Yuan, D. Ding, D. L. Kong, B. Liu, *Adv. Mater.* **2017**, 29, 1700548.
- [10] A. Almeida, M. A. F. Faustino, J. P. C. Tomé, *Future Med. Chem.* **2015**, 7, 1221.
- [11] G. X. Feng, C. J. Zhang, X. M. Lu, B. Liu, *ACS Omega* **2017**, 2, 546.
- [12] J. Mei, Y. Hong, J. W. Y. Lam, B. Z. Tang, *Adv. Mater.* **2014**, 26, 5429.
- [13] D. Wang, H. F. Su, R. T. K. Kwok, G. G. Shan, A. C. S. Leung, M. M. S. Lee, H. H. Y. Sung, I. D. Williams, J. W. Y. Lam, B. Z. Tang, *Adv. Funct. Mater.* **2017**, 27, 1704039.
- [14] Y. Hong, J. W. Y. Lam, B. Z. Tang, *Chem. Soc. Rev.* **2011**, 40, 5361.
- [15] E. G. Zhao, Y. N. Hong, S. J. Chen, C. W. T. Leung, C. Y. K. Chan, R. T. K. Kwok, J. W. Y. Lam, B. Z. Tang, *Adv. Healthcare Mater.* **2014**, 3, 88.
- [16] S. Xie, S. Manuguri, G. Proietti, J. Romson, Y. Fu, A. K. Inge, B. Wu, Y. Zhang, D. Häll, O. Ramström, M. Yan, *Proc. Acad. Natl. Sci. USA* **2017**, 114, 8464.
- [17] J. Mei, Y. H. Huang, H. Tian, *ACS Appl. Mater. Inter.* **2018**, 10, 12217.
- [18] E. G. Zhao, Y. L. Chen, H. Wang, S. J. Chen, J. W. Y. Lam, C. W. T. Leung, Y. N. Hong, B. Z. Tang, *ACS Appl. Mater. Inter.* **2015**, 7, 7180.
- [19] G. X. Feng, Y. Y. Yuan, H. Fang, R. Y. Zhang, B. G. Xing, G. X. Zhang, D. Q. Zhang, B. Liu, *Chem. Commun.* **2015**, 51, 12490.
- [20] Y. H. Wu, Q. X. Chen, Q. Y. Li, H. G. Lu, X. S. Wu, J. B. Ma, H. Gao, *J. Mater. Chem. B* **2016**, 4, 6350.
- [21] S. Chen, Q. X. Chen, Q. Y. Li, J. X. An, P. Sun, J. B. Ma, H. Gao, *Chem. Mater.* **2018**, 30, 1782.
- [22] A. Kamal, S. F. Adil, J. R. Tamboli, B. Siddardh, U. S. N. Murthy, *Letts. Drug Des. Discov.* **2009**, 6, 201.
- [23] S. A. F. Rostom, H. M. A. Ashour, H. A. A. E. Razik, A. E. F. H. A. E. Fattah, N. N. El-Din, *Bioorg. Med. Chem. Lett.* **2009**, 17, 2410.
- [24] Y. Y. Zhang, C. H. Zhou, *Bioorg. Med. Chem. Lett.* **2011**, 21, 4349.
- [25] Z. Zhao, S. M. Gao, X. Y. Zheng, P. F. Zhang, W. T. Wu, R. T. K. Kwok, Y. Xiong, N. L. C. Leung, Y. C. Chen, X. K. Gao, J. W. Y. Lam, B. Z. Tang, *Adv. Funct. Mater.* **2018**, 28, 1705609.
- [26] Z. Zhao, Z. L. Wang, Y. B. Hu, X. D. Yang, H. X. Li, X. K. Gao, D. B. Zhu, *J. Org. Chem.* **2013**, 78, 12214.
- [27] W. Qin, K. Li, G. X. Feng, M. Li, Z. Y. Yang, B. Liu, B. Z. Tang, *Adv. Funct. Mater.* **2014**, 24, 635.
- [28] D. Ding, K. Li, B. Liu, B. Z. Tang, *Acc. Chem. Res.* **2013**, 46, 2441.
- [29] J. Liang, B. Z. Tang, B. Liu, *Chem. Soc. Rev.* **2015**, 44, 2798.
- [30] F. Hu, Y. Y. Huang, G. X. Zhang, R. Zhao, H. Yang, D. Q. Zhang, *Anal. Chem.* **2014**, 86, 7987.
- [31] E. G. Zhao, H. Q. Deng, S. J. Chen, Y. N. Hong, C. W. T. Leung, J. W. Y. Lam, B. Z. Tang, *Chem. Commun.* **2014**, 50, 14451.
- [32] W. B. Wu, D. Mao, S. D. Xu, S. L. Ji, F. Hu, D. Ding, D. L. Kong, B. Liu, *Mater. Horiz.* **2017**, 4, 1110.
- [33] T. Wu, A. C. McCandlish, L. S. Gronenberg, S. S. Chng, T. J. Silhavy, D. Kahne, *Proc. Acad. Natl. Sci. USA* **2006**, 103, 11754.
- [34] M. A. Pereira, M. A. F. Faustino, J. P. C. Tomé, M. G. P. M. S. Neves, J. A. C. Tomé, J. A. S. Cavaleiro, Â. Cunha, A. Almeida, *Photochem. Photobiol. Sci.* **2014**, 13, 680.
- [35] D. R. Storm, K. S. Rosenthal, P. E. Swanson, *Annu. Rev. Biochem.* **1977**, 46, 723.
- [36] W. Chin, G. S. Zhong, Q. Q. Pu, C. Yang, W. Y. Lou, P. F. D. Sessions, B. Periaswamy, A. Lee, Z. C. Liang, X. Ding, S. J. Gao, C. W. H. Chu, S. Bianco, C. Bao, Y. W. Tong, W. M. Fan, M. Wu, J. L. Hedrick, Y. Y. Yang, *Nat. Commun.* **2018**, 9, 917.
- [37] W. L. Garner, *Plast. Reconstr. Surg.* **1998**, 102, 135.
- [38] D. Jana, B. K. Ghorai, *Tetrahedron Lett.* **2012**, 53, 6838.
- [39] Y. Y. Zhao, Y. Tian, Y. Cui, W. W. Liu, W. S. Ma, X. Y. Jiang, *J. Am. Chem. Soc.* **2010**, 132, 12349.